

Stability and Instability Criteria for Idealized Precipitating Hydrodynamics

GERARDO HERNANDEZ-DUENAS

*Instituto de Matemáticas Campus Juriquilla, Universidad Nacional Autónoma de México,
Juriquilla, Querétaro, México*

LESLIE M. SMITH

*Department of Mathematics, and Department of Engineering Physics, University
of Wisconsin–Madison, Madison, Wisconsin*

SAMUEL N. STECHMANN

*Department of Mathematics, and Department of Atmospheric and Oceanic Sciences,
University of Wisconsin–Madison, Madison, Wisconsin*

(Manuscript received 23 October 2014, in final form 12 February 2015)

ABSTRACT

A linear stability analysis is presented for fluid dynamics with water vapor and precipitation, where the precipitation falls relative to the fluid at speed V_T . The aim is to bridge two extreme cases by considering the full range of V_T values: (i) $V_T = 0$, (ii) finite V_T , and (iii) infinitely fast V_T . In each case, a saturated precipitating atmosphere is considered, and the sufficient conditions for stability and instability are identified. Furthermore, each condition is linked to a thermodynamic variable: either a variable θ_s , which denotes the saturated potential temperature, or the equivalent potential temperature θ_e . When V_T is finite, separate sufficient conditions are identified for stability versus instability: $d\theta_e/dz > 0$ versus $d\theta_s/dz < 0$, respectively. When $V_T = 0$, the criterion $d\theta_s/dz = 0$ is the single boundary that separates the stable and unstable conditions; and when V_T is infinitely fast, the criterion $d\theta_e/dz = 0$ is the single boundary. Asymptotics are used to analytically characterize the infinitely fast V_T case, in addition to numerical results. Also, the small- V_T limit is identified as a singular limit; that is, the cases of $V_T = 0$ and small V_T are fundamentally different. An energy principle is also presented for each case of V_T , and the form of the energy identifies the stability parameter: either $d\theta_s/dz$ or $d\theta_e/dz$. Results for finite V_T have some resemblance to the notion of conditional instability: separate sufficient conditions exist for stability versus instability, with an intermediate range of environmental states where stability or instability is not definitive.

1. Introduction

Various notions of stability and instability have been valuable in understanding moist convection. For example, two common types are potential instability and conditional instability. Furthermore, conditional instability can be defined in multiple ways, in terms of lapse rates or in terms of parcel buoyancy (Schultz et al. 2000; Sherwood 2000), and it can be further modified to include or neglect various aspects of moist convection

(Xu and Emanuel 1989; Williams and Renno 1993; Emanuel 1994).

As their definitions come in a multitude of forms, stability and instability can be investigated using a multitude of approaches. The present paper utilizes a set of equations for idealized precipitating fluid dynamics. The equations include moist thermodynamics in a simplified form, which facilitates analytical calculations; at the same time, the equations also have a representation of the fall speed of precipitation, which adds an extra element of realism beyond traditional analytical approaches. To put this approach in perspective, we next summarize some broader ultimate goals and some of the approaches used in their pursuit. As is the case for all approaches, the present approach falls short of a

Corresponding author address: Gerardo Hernandez-Duenas, Instituto de Matemáticas Campus Juriquilla, Universidad Nacional Autónoma de México, 3001 Boulevard Juriquilla, Juriquilla, Queretaro 76230, Mexico.
E-mail: hernandez@im.unam.mx

complete answer but nevertheless provides an interesting perspective.

The ultimate question concerning deep moist convection can perhaps be summarized as follows: Given an unsaturated profile of the environmental thermodynamic state [e.g., potential temperature $\theta(z)$ and water vapor mixing ratio $q_v(z)$], what is the probability that cumulus convection and/or precipitation will form? Refinements to this question could include further details, such as a measure of the convective intensity in terms of cloud-top height or maximum vertical velocity. In the end, because of the complexity of the question, the ultimate answer will likely not be a simple yes or no answer but an answer in terms of probabilities. As such, this question could potentially be answered probabilistically using a numerical forecasting perspective, although at considerable computational expense. Instead, investigations have traditionally sought a simpler answer in terms of environmental lapse rates and/or single-column models of plumes or rising parcels (Xu and Emanuel 1989; Williams and Renno 1993; Emanuel 1994; Schultz et al. 2000; Sherwood 2000), which perhaps are not as accurate as the numerical forecasting perspective, but which are advantageous for their conceptual simplicity.

Difficulties abound in this ultimate question. Two examples are the following. First, a nonlinear switch arises between the unsaturated and saturated states. As a result, the buoyancy has a different form in the unsaturated and saturated states (Stevens 2005). Second, the formulas for cloud microphysics and precipitation are mathematically intractable and, hence, amenable only to numerical computations. More specifically, these equations typically take a complex form involving nonlinear switches (i.e., the Heaviside function) and polynomial nonlinearities (Grabowski and Smolarkiewicz 1996; Seifert and Beheng 2001, 2006; Morrison and Grabowski 2008b). Consequently, the ultimate question is perhaps impossible to answer analytically precisely as stated.

To circumvent these difficulties, various simplifications are traditionally employed. For example, one simplification is to ignore the nonhydrostatic pressure gradient force, which is essentially tantamount to ignoring hydrodynamics altogether. Such an assumption leads to the commonly used parcel dynamics and parcel theory for analyzing atmospheric stability (Xu and Emanuel 1989; Williams and Renno 1993; Xu and Randall 2001). As another example, one could ignore the effect of condensate loading (or hydrometeor drag) on buoyancy by assuming a pseudoadiabatic thermodynamic process rather than a reversible process. As a last example, in some analytical theories it is necessary to assume saturated

conditions in order to circumvent the nonlinear switch between the unsaturated and saturated states.

Analytical theories typically neglect the rainfall velocity V_T . An exception is the work of Emanuel (1986), who considered the linear stability of an idealized saturated atmosphere with precipitation that falls at speed V_T . Emanuel (1986) showed that upright or tilted modes could exist and be unstable. Further work by Bretherton (1987b) examined the same model and focused on the limit of infinitely small spatial scales.

The use of finite V_T helps bridge two extreme cases: those that ignore V_T and those that assume V_T is infinitely fast (e.g., with the result that liquid water is removed immediately when it forms in a rising parcel). The work of Emanuel (1986) presents illuminating results in this direction, but its main aim is geared toward the dynamical consequences of finite V_T , such as tilted updrafts of propagating squall lines. In the present paper, the focus is not on the detailed structure of the unstable eigenmodes but rather on the atmospheric conditions for guaranteeing stability or instability. In other words, one aim here is to put the finite- V_T case in the context of lapse rate criteria for moist atmospheric stability and instability.

The main results presented here consider three possible cases: (i) the case $V_T = 0$, (ii) finite V_T , and (iii) the limit $V_T \rightarrow \infty$. For finite V_T , it is shown that two separate conditions arise for instability versus stability: the sufficient condition for instability ($d\theta_s/dz < 0$) is determined by a variable $\theta_s = \theta_e - \theta_0 q_t$ that we call the saturated potential temperature, whereas the equivalent potential temperature gradient provides a sufficient condition for stability ($d\theta_e/dz > 0$). This is in contrast to the previously derived case of $V_T = 0$, where a single quantity ($d\theta_s/dz$) provides the sufficient conditions for both stability and instability. Two other interesting results also arise from analyzing cases (i)–(iii): the limit $V_T \rightarrow 0$ is shown to be a singular limit (i.e., the case of small V_T is fundamentally different from the case of $V_T = 0$), and the limit $V_T \rightarrow \infty$ leads to stability and instability conditions determined by a single quantity, the equivalent potential temperature gradient $d\theta_e/dz$. Finally, all of these conditions are related to the energy principle that arises in each case.

In this paper, saturated conditions will be the focus. As such, the processes leading to saturation are not addressed, and the approach falls short of the goals in the ultimate question described above. Nevertheless, several realistic features are included in the hydrodynamic theory here but neglected in typical parcel theories; this includes the nonhydrostatic pressure gradient force (and hence hydrodynamics) and finite rainfall velocity V_T .

The nonlinear version of the model was described by Hernandez-Duenas et al. (2013). In that work, the

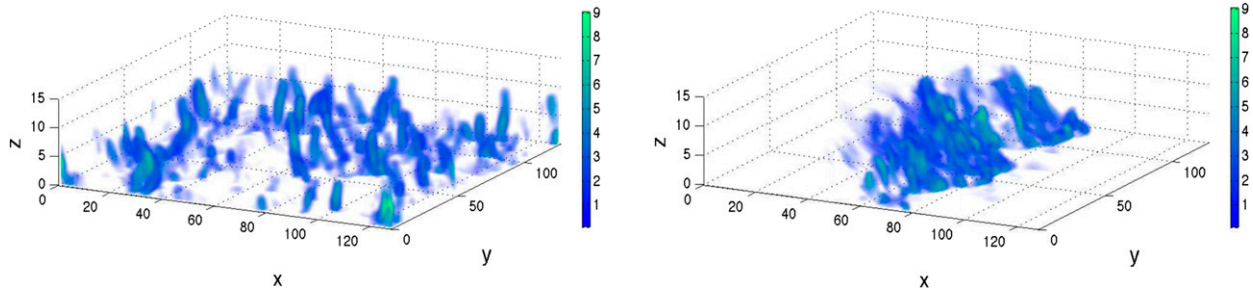


FIG. 1. Contours of rainwater q_r (g kg^{-1}) for two numerical simulations using the nonlinear FARE model. The two cases are (left) scattered convection and (right) a squall line. Reprinted with permission from Hernandez-Duenas et al. (2013).

model was named the Fast Autoconversion and Rain Evaporation (FARE) model because of the assumption of fast microphysical time scales. In many ways, the nonlinear FARE model is similar to the earlier models of Seitter and Kuo (1983), Majda et al. (2010), Sukhatme et al. (2012), and Deng et al. (2012), all of which employ an assumption of infinitely fast autoconversion: small cloud droplets instantaneously collide and amalgamate to form large rain drops. Short- and long-time, two-dimensional simulations with fast autoconversion were studied, respectively, in Seitter and Kuo (1983) and Sukhatme et al. (2012). To investigate cyclogenesis, Majda et al. (2010) considered fast autoconversion, together with a weak temperature gradient (WTG) approximation, and later Deng et al. (2012) relaxed WTG to allow for the effects of inertia-gravity waves. What distinguishes the FARE model from these earlier models is the additional assumption of fast rain evaporation: if rainwater falls into unsaturated air, it is instantaneously evaporated until saturation is reached or until all rainwater is depleted. Hernandez-Duenas et al. (2013) show that the FARE model can reproduce the basic regimes of precipitating turbulent convection: scattered convection in an environment of low wind shear and a squall line in an environment with strong wind shear. These two cases are reproduced here in Fig. 1. While a linearized version of the FARE model is used in the present paper, these nonlinear results lend confidence to the idealizations used in the model.

The rest of the paper is organized as follows. In section 2, the nonlinear equations of the FARE model are described, followed by the linearized models for saturated and unsaturated regions. Energy principles are also presented for each case, and some initial insight into stability conditions can be gleaned from the form of the energy. Section 3 describes the linear stability analysis for three cases: (i) the case $V_T = 0$, (ii) finite V_T , and (iii) the limit $V_T \rightarrow \infty$. In section 4, results of the infinitely fast V_T case are obtained analytically using asymptotics. A concluding discussion is presented in section 5.

2. The FARE model and energy

a. Background and derivation

A typical cloud-resolving model (CRM) would be based on the equations of motion for a compressible fluid or on the anelastic approximation filtering acoustic waves but allowing for vertical motions of depth comparable to the density scale height (Ogura and Phillips 1962; Lipps and Hemler 1982). The thermodynamics would be as comprehensive as possible, including multiple phases of water (vapor, cloud water, rain, snow, ice, hail, graupel, etc.), and often modeling the detailed cloud microphysics of individual water droplets (Grabowski and Smolarkiewicz 1996; Seifert and Beheng 2001, 2006; Grabowski and Morrison 2008). Although this comprehensive approach is necessary for weather prediction, some physical insights into the fundamental processes of moist convection may be more easily extracted from simplified systems. For example, in the context of organized convection, valuable insights have been gained from simplified perspectives (Moncrieff and Green 1972; Moncrieff and Miller 1976; Moncrieff 1981; Emanuel 1986; Moncrieff 1992; Garner and Thorpe 1992; Fovell and Tan 2000). In a similar simplified spirit, although not aimed at organized convection, we here consider the minimal FARE model, based on Boussinesq fluid dynamics (Spiegel and Veronis 1960) and simplified thermodynamics retaining only water vapor and precipitating rainwater. The reduction supports a system of equations with conservation of an equivalent potential temperature, as well as conservation of total water and rainwater potential temperature in the limit of vanishing rainfall speed. Preservation of these basic conservation laws is presumably key to model utility in the absence of detailed physics. When the system is written in terms of total water and equivalent potential temperature (or rainwater potential temperature), then the source terms for condensation and evaporation do not appear explicitly, thus eliminating the need for closure models of phase changes. The FARE model is fully three-dimensional

(3D) and, in principle, able to resolve turbulent motions at small scales. The Boussinesq approximation for shallow vertical motions is, of course, unrealistic for the real atmosphere, but our numerical computations have demonstrated that some regimes of convective organization (scattered convection and squall line formation) are supported by a Boussinesq atmosphere; thus, FARE's minimal nature appears to outweigh its restrictions for our purposes.

The limit of fast autoconversion eliminates the need to carry cloud water as a variable as well as the need to model autoconversion of cloud water to rainwater. On the other hand, autoconversion occurs on a time scale on the order of minutes, whereas the condensation time scale is on the order of seconds (Rogers and Yau 1989; Houze 1993; Morrison and Grabowski 2008a). Thus, it is sensible to also assume fast condensation. As a further simplification, Hernandez-Duenas et al. (2013) proposed an assumption of fast evaporation of rainwater; such an assumption differs from the rain evaporation model of Seitter and Kuo (1983). Taken together, these simplifications form the model denoted FARE, with fast condensation and fast rain evaporation in addition to fast autoconversion. In such a model, there is no possibility for supersaturation, because the water vapor is instantaneously relaxed back toward the saturation profile. Furthermore, rainwater cannot exist in unsaturated air, because it is instantaneously evaporated until water vapor is increased to the saturation level.

The FARE model may be written as

$$\frac{D\mathbf{u}}{Dt} = -\nabla p + \hat{\mathbf{k}}g \left(\frac{\theta}{\theta_o} + \varepsilon_o q_v - q_r \right), \quad \nabla \cdot \mathbf{u} = 0 \quad \text{and} \quad (1)$$

$$\frac{D\theta}{Dt} = \frac{L}{c_p} (C_d - E_r),$$

$$\frac{Dq_v}{Dt} = -C_d + E_r, \quad \frac{Dq_r}{Dt} - V_T \frac{\partial q_r}{\partial z} = C_d - E_r, \quad (2)$$

where $D/Dt = \partial_t + \mathbf{u} \cdot \nabla$ is the material derivative, $\mathbf{u}(\mathbf{x}, t)$ is the 3D velocity vector with components (u, v, w) , $\theta(\mathbf{x}, t)$ is the potential temperature, $p(\mathbf{x}, t)$ is the pressure, and $q_v(\mathbf{x}, t)$ and $q_r(\mathbf{x}, t)$ denote the mixing ratios of water vapor and rainwater, respectively. The source terms C_d and E_r represent phase changes of water substance, respectively: condensation C_d of water vapor to form rainwater, and evaporation E_r of rainwater to form water vapor. The unit vector $\hat{\mathbf{k}}$ is the direction of gravity (not to be confused with the wavevector \mathbf{k} introduced below). The rainfall speed V_T is normally in the range $0 \leq V_T \leq 10 \text{ m s}^{-1}$ [see Table 8.1 in Rogers and Yau (1989)] and will be allowed to vary in the stability analysis of section 3. The

other parameters will be fixed at standard values: the latent heat factor $L = 2.5 \times 10^6 \text{ J kg}^{-1}$, the specific heat $c_p = 10^3 \text{ J kg}^{-1} \text{ K}^{-1}$, the ratio of gas constants $R_v/R_d = \varepsilon_o + 1 = 1.6$, the acceleration of gravity $g = 9.81 \text{ m s}^{-2}$, and the reference potential temperature $\theta_o = 300 \text{ K}$.

In the limit of fast condensation and evaporation, the source terms C_d and E_r maintain the following constraints and are actually defined so as to maintain these constraints:

$$\text{either } q_v < q_{vs}(z), \quad q_r = 0 \quad (\text{unsaturated}) \quad (3)$$

$$\text{or } q_v = q_{vs}(z), \quad q_r \geq 0 \quad (\text{saturated}), \quad (4)$$

where $q_{vs}(z)$ is an approximation for the saturation water vapor profile (Majda et al. 2010; Deng et al. 2012; Hernandez-Duenas et al. 2013). The formulation (3) and (4) is commonly used in CRMs (Grabowski and Smolarkiewicz 1996) and in more idealized models of moist convection (Bretherton 1987a; Pauluis and Schumacher 2010), but with q_c rather than q_r . Because of constraints (3) and (4), only two thermodynamic variables are needed, instead of the three variables θ , q_v , and q_r .

Here, we choose to rewrite FARE in terms of the mixing ratio of total water $q_t = q_v + q_r$ and the (conserved) equivalent potential temperature $\theta_e = \theta + (L/c_p)q_v$, which is a linearization of the actual potential temperature $\theta \exp[Lq_v/(c_p T)]$ (Stevens 2005). We use the relations

$$q_v = \min(q_t, q_{vs}), \quad q_r = \max(0, q_t - q_{vs}), \quad (5)$$

which follow from (3) and (4). Next, the last two equations of (2) are used to write the combined source terms

$$C_d - E_r = \begin{cases} 0, & \text{if } q_t \leq q_{vs} \\ -wdq_{vs}(z)/dz, & \text{if } q_t > q_{vs} \end{cases}.$$

Finally, combining the first and third equations of (2) leads to

$$\frac{D\mathbf{u}}{Dt} = -\nabla p + \hat{\mathbf{k}}g \left[\frac{\theta_e}{\theta_o} + \left(\varepsilon_o - \frac{L}{c_p \theta_o} \right) q_v - q_r \right], \quad (6)$$

$$\nabla \cdot \mathbf{u} = 0 \quad \text{and}$$

$$\frac{D\theta_e}{Dt} = 0, \quad \frac{Dq_t}{Dt} - V_T \frac{\partial q_r}{\partial z} = 0. \quad (7)$$

Note that the total water q_t is conserved when $V_T = 0$. In a dry or unsaturated atmosphere, there is additional conservation of the (linearized) virtual potential temperature $\theta_v = \theta_o(\theta/\theta_o + \varepsilon_o q_v - q_r)$, but the same will not be true for saturated regions.

When using the FARE model, water vapor and rainwater are computed from total water q_t using (5). Thus,

the model consists of (6) and (7), together with (5) and the relation $\theta = \theta_e - (L/c_p)q_v$. Note that nonlinear switches are still present in (5), presenting a challenge for analysis. Here, we focus on linear analysis of completely unsaturated or completely saturated regions far enough away from the threshold for nonlinear effects of phase changes.

Analogously to Hernandez-Duenas et al. (2013), one can show that the FARE model has an energy consistency equation:

$$\frac{\partial}{\partial t} \left(\frac{\mathbf{u} \cdot \mathbf{u}}{2} + \Pi \right) + \nabla \cdot \left[\mathbf{u} \left(\frac{\mathbf{u} \cdot \mathbf{u}}{2} + \Pi + p \right) \right] - \frac{\partial}{\partial z} [V_T g(z-a)q_r] = -V_T g q_r, \quad (8)$$

where the potential energy Π is given by (Vallis 2006; Pauluis 2008)

$$\Pi(\theta_e, q_t, z) = - \int_a^z \frac{g}{\theta_o} \theta_v(\theta_e, q_t, \eta) d\eta, \quad (9)$$

and the linear virtual potential temperature θ_v as a function of θ_e , q_t , and z is given by

$$\theta_v = \theta_v(\theta_e, q_t, z) = \theta_e - \theta_o q_t + \theta_o \left(\varepsilon_o - \frac{L}{c_p \theta_o} + 1 \right) \min[q_t, q_{vs}(z)]. \quad (10)$$

The integration in (9) assumes θ_e and q_t are fixed, and a is an arbitrary reference height satisfying $q_{vs}(a) = 0$. The energy sink term involving the rainfall speed V_T is consistent with physical interpretation of $-gq_r$ as a frictional drag force on the surrounding air when $V_T > 0$. The energy [(8)] involves the total dynamic and thermodynamics field variables and is valid in general, including across phase changes. In a later section on energetics, we will assume a quiescent background environment that is either unsaturated or saturated, away from phase changes. For these environments, (8) takes a simpler form, with Π given by an explicit quadratic function of fluctuations from the background thermodynamic state and the pressure redefined to absorb background thermodynamic fields. It is important to note that there is a direct pathway from (8) to (28) below, but the algebra is rather tedious and so will be omitted for brevity.

b. The linearized equations

To perform the linear stability analysis, we consider perturbations from an unsaturated or saturated resting state. Thus, all thermodynamical variables are decomposed into a background function of altitude and fluctuating part according to $(\cdot) = (\cdot) + (\cdot)'$. For a more

TABLE 1. Definition of thermodynamic quantities used throughout this paper.

Quantity	Definition
Total water mixing ratio	q_t
Water vapor mixing ratio	$q_v = \min(q_t, q_{vs})$
Rainwater mixing ratio	$q_r = \max(q_t - q_{vs}, 0)$
Potential temperature	θ
Virtual potential temperature	$\theta_v = \theta + \theta_o(\varepsilon_o q_v - q_r)$
Buoyancy frequency squared, unsaturated	$\Gamma_v = (g/\theta_o)d\theta_v/dz$
Saturated potential temperature	$\theta_s = \theta_e - \theta_o q_t$
Buoyancy frequency squared, $V_T = 0$	$\Gamma_s = (g/\theta_o)d\theta_s/dz$
Equivalent potential temperature	$\theta_e = \theta + (L/c_p)q_v$
Buoyancy frequency squared, $V_T \rightarrow \infty$	$\Gamma_e = (g/\theta_o)d\theta_e/dz$
Rainwater potential temperature	$\theta_r = \theta - (L/c_p)q_r$

general analysis, one could also consider a height-dependent background horizontal velocity, but the rest state $\tilde{\mathbf{u}} = 0$ allows for explicit calculation of linear eigenmodes using periodic boundary conditions. For simplicity, the background potential temperature will be linear $\tilde{\theta} = \theta_o + Bz$ with $\theta_o = 300$ K. As mentioned above, the FARE model also assumes a saturation water vapor $q_{vs}(z)$ that is a function of height only. Our minimal modeling approach allows us to treat the background potential temperature gradient B as independent from the gradient of the saturation profile $dq_{vs}/dz = B_{vs}$, both taken to be constant. Unless otherwise stated, we fix the value of $B = 3$ K km⁻¹ corresponding to a standard Brunt-Väisälä frequency of $N = \sqrt{gB/\theta_o} \approx 10^{-2}$ s⁻¹ and then vary B_{vs} .

As will be shown, different (in)stability parameters and (in)stability boundaries arise for the different cases: unsaturated regions; saturated nonprecipitating regions with $V_T = 0$; saturated precipitating regions with $V_T > 0$; and saturated precipitating regions with $V_T \rightarrow \infty$. The (in)stability parameters Γ_v , Γ_s , and Γ_e involve background gradients of the thermodynamic variables and are defined in Table 1.

1) UNSATURATED REGIONS

In unsaturated regions of the atmosphere with $q_r = 0$, the linearized FARE model may be written as

$$\frac{\partial \mathbf{u}'}{\partial t} = -\nabla \phi + \mathbf{k}g \left(\frac{\theta'}{\theta_o} + \varepsilon_o q_v' \right), \quad \nabla \cdot \mathbf{u}' = 0 \quad \text{and} \quad (11)$$

$$\frac{\partial \theta'}{\partial t} + Bw' = 0, \quad \frac{\partial q_v'}{\partial t} + w' \frac{d\tilde{q}_v}{dz} = 0, \quad (12)$$

where the background virtual potential temperature has been absorbed into the modified pressure such that $\phi = p - (g/\theta_o) \int_0^z \tilde{\theta}_v(\eta) d\eta$, with $\tilde{\theta}_v = \theta_o(\tilde{\theta}/\theta_o + \varepsilon_o \tilde{q}_v)$.

One can directly compare the unsaturated moist and dry dynamics in the sense that the buoyancy $b = (g/\theta_o)\theta'_v = g(\theta'/\theta_o + \varepsilon_o q'_v)$ here includes water vapor but the material derivatives of both θ and q_v are zero, as in the dry Bousinesq dynamics. Rescaling and adding the two equations in (12) gives $D\theta_v/Dt = 0$ or, equivalently,

$$\frac{Db}{Dt} = -\Gamma_v w', \quad \Gamma_v = \frac{g}{\theta_o} \frac{d\tilde{\theta}_v}{dz} = \frac{gB}{\theta_o} + g\varepsilon_o \frac{d\tilde{q}_v}{dz}. \quad (13)$$

As shown below, the stability condition is dictated by the gradient Γ_v , which involves the negative slope $d\tilde{q}_v/dz$. The presence of moisture will introduce instabilities if $d\tilde{q}_v/dz$ is negative enough, even if the atmosphere is stably stratified with $B > 0$. However, we note that for $B = 3 \text{ K km}^{-1}$, the instability interface occurs at $d\tilde{q}_v/dz = -16.67 \text{ g kg}^{-1} \text{ km}^{-1}$. For an atmosphere of height 15 km, the difference in moisture between the top and bottom would be more than 200 g kg^{-1} , which is not a realistic scenario.

2) SATURATED REGIONS

In completely saturated regions of the FARE atmosphere, the mixing ratio of water vapor is equal to the saturation profile $q_v = q_{vs}(z)$; thus, it follows that the rainwater is given by $q_r = q_t - q_{vs}$ and $q'_r = q'_t$. To ensure a steady-state background, we choose a constant background rain $\tilde{q}_r = q_{r,o} = \tilde{q}_t - q_{vs}$ with $d\tilde{q}_r/dz = 0$ and $d\tilde{q}_t/dz = dq_{vs}/dz = B_{vs}$. Then the linearized version of (6) and (7) may be written as

$$\frac{\partial \mathbf{u}'}{\partial t} = -\nabla \phi + \hat{\mathbf{k}}g \left(\frac{\theta'_e}{\theta_o} - q'_r \right), \quad \nabla \cdot \mathbf{u}' = 0 \quad \text{and} \quad (14)$$

$$\frac{g}{\theta_o} \frac{\partial \theta'_e}{\partial t} + \Gamma_e w' = 0, \quad g \frac{\partial q'_r}{\partial t} + (\Gamma_e - \Gamma_s) w' - V_T g \frac{\partial q'_r}{\partial z} = 0, \quad (15)$$

where

$$\Gamma_e = \frac{g}{\theta_o} \frac{d\tilde{\theta}_e}{dz} = \frac{g}{\theta_o} \left(B + \frac{L}{c_p} B_{vs} \right),$$

$$\Gamma_s = \frac{g}{\theta_o} \frac{d(\tilde{\theta}_e - \theta_o \tilde{q}_t)}{dz} = \frac{g}{\theta_o} \left(B + \frac{L}{c_p} B_{vs} \right) - gB_{vs}, \quad \text{and} \quad (16)$$

$$\Gamma_e - \Gamma_s = g \frac{d\tilde{q}_t}{dz} = gB_{vs}. \quad (17)$$

The modified pressure is $\phi = p - (g/\theta_o) \int_0^z \tilde{\theta}_v(\eta) d\eta$ with $\tilde{\theta}_v = \theta_o(\tilde{\theta}/\theta_o + \varepsilon_o q_{vs} - q_{r,o})$. Given the appearance of Γ_s

in (16), it is sensible to define a variable $\theta_s = \theta_e - \theta_o q_t$, which we will call the saturated potential temperature and which will be an important variable for linear (in)stability of a saturated environment. The parameter Γ_e is positive when the background of the equivalent potential temperature increases with height, whereas the difference $\Gamma_s - \Gamma_e = -gd\tilde{q}_t/dz = -gB_{vs}$ is positive when the moisture background decreases with height (always assumed here). In the second equation of (15), the term involving V_T leads to nonconservation of the virtual potential temperature θ_v ; consequently, as shown next, the linearized energy equation takes a form different from the cases of unsaturated and nonprecipitating saturated environments, both of which have the same form as the dry dynamics.

c. Energetics

In the following sections on energetics, we consider the nonlinear system in various regimes: unsaturated, saturated with $V_T = 0$, and saturated with $V_T > 0$. We choose to decompose the thermodynamics variables into background and fluctuations in order to extract the stability boundaries defined in terms of background gradients Γ_v , Γ_s , and Γ_e of thermodynamics quantities.

1) ENERGY EQUATION IN UNSATURATED REGIONS

With $\theta = \tilde{\theta} + \theta'$ and $q_v = \tilde{q}_v + q'_v$, the nonlinear dynamics in unsaturated regions takes the form

$$\frac{D\mathbf{u}}{Dt} = -\nabla \phi + \hat{\mathbf{k}}g \left(\frac{\theta'}{\theta_o} + \varepsilon_o q'_v \right), \quad \nabla \cdot \mathbf{u} = 0 \quad \text{and} \quad (18)$$

$$\frac{D\theta'}{Dt} + Bw = 0, \quad \frac{Dq'_v}{Dt} + w \frac{d\tilde{q}_v}{dz} = 0. \quad (19)$$

It follows that the kinetic $\|\mathbf{u}\|^2/2$ and ‘‘potential’’ $b^2/(2\Gamma_v)$ energies satisfy the equations

$$\frac{D}{Dt} \left(\frac{1}{2} \|\mathbf{u}\|^2 \right) = -\nabla \cdot (\mathbf{u}\phi) + wb, \quad \frac{D}{Dt} \left(\frac{b^2}{2\Gamma_v} \right) = -wb. \quad (20)$$

Here, $b = g(\theta'/\theta_o + \varepsilon_o q'_v)$ is the buoyancy in unsaturated regions. Exchange of kinetic and potential energy is possible as a result of the wb term in each equation, and the energy equation in conservation form is obtained after adding the two equations in (20):

$$\frac{\partial E}{\partial t} + \nabla \cdot [\mathbf{u}(E + \phi)] = 0, \quad E = \frac{1}{2} \|\mathbf{u}\|^2 + \frac{b^2}{2\Gamma_v}. \quad (21)$$

From the form of this energy, it is clear that a sufficient condition for stability is $\Gamma_v > 0$.¹ What is not clear from the energy alone is the sufficient condition for instability, although it is well known to be $\Gamma_v < 0$ from linear stability analysis analogous to the dry dynamics (Vallis 2006).

2) ENERGY EQUATION IN SATURATED REGIONS WITH $V_T = 0$

With $\theta_e = \tilde{\theta}_e + \theta'_e$, $q_r = \tilde{q}_r + q'_r$, the nonlinear dynamics in saturated regions takes the form

$$\frac{D\mathbf{u}}{Dt} = -\nabla\phi + \hat{\mathbf{k}}g\left(\frac{\theta'_e}{\theta_o} - q'_r\right), \quad \nabla \cdot \mathbf{u} = 0 \quad \text{and} \quad (22)$$

$$\frac{g}{\theta_o} \frac{D\theta'_e}{Dt} + \Gamma_e w = 0, \quad g \frac{Dq'_r}{Dt} + (\Gamma_e - \Gamma_s)w - V_T g \frac{\partial q'_r}{\partial z} = 0. \quad (23)$$

Setting $V_T = 0$ and subtracting the two equations in (23), one finds

$$\frac{D\mathbf{u}}{Dt} = -\nabla\phi + \hat{\mathbf{k}}b, \quad \nabla \cdot \mathbf{u} = 0, \quad \frac{Db}{Dt} = -\Gamma_s w, \quad (24)$$

with buoyancy $b = (g/\theta_o)\theta'_e = g(\theta'_e/\theta_o - q'_r)$. Notice that the equation for the buoyancy in (24) has the same form as (13) for unsaturated environments, with Γ_v in (13) replaced by Γ_s . Defining the energy

$$E = \frac{1}{2}\|\mathbf{u}\|^2 + \frac{b^2}{2\Gamma_s} \quad (25)$$

leads to

$$\frac{\partial E}{\partial t} + \nabla \cdot [\mathbf{u}(E + \phi)] = 0. \quad (26)$$

From the form of the energy in (25), it is clear that a sufficient condition for stability is $\Gamma_s > 0$. What is not immediately clear from (25) alone is a sufficient condition for instability. However, since the mathematical form of (24) is the same as (13) (i.e., the unsaturated case, but with Γ_v replaced by Γ_s), it follows that $\Gamma_s < 0$ is a sufficient condition for instability. Taking this mathematical equivalence further, explicit expressions for the

¹ Since energy is conserved, the condition $\Gamma_v > 0$ ensures that both kinetic and potential energies are positive and thus remain bounded assuming appropriate boundary conditions. On the other hand, if $\Gamma_v < 0$, the oppositely signed kinetic and potential energies can grow without bound while the total energy remains fixed, indicating the possibility of instability.

frequencies of the linear eigenmodes are $\sigma^\pm = \pm(k_h/k)\Gamma_s^{1/2}$, where $\mathbf{k} = (k_x, k_y, k_z)$ is the wavevector, $k = \sqrt{k_x^2 + k_y^2 + k_z^2}$ is the wavenumber, and $k_h = \sqrt{k_x^2 + k_y^2}$ is the horizontal equivalent.

3) ENERGY EQUATION IN SATURATED REGIONS WITH $V_T > 0$

The quantity (25) is not conserved if $V_T > 0$; hence, a different form is required in this case. To arrive at an energy conservation principle for $V_T > 0$ requires a separate scaling for each term in the buoyancy $b = g(\theta'_e/\theta_o - q'_r)$. Defining a precipitating energy

$$E_p = \frac{1}{2}\|\mathbf{u}\|^2 + \frac{(g\theta'_e/\theta_o)^2}{2\Gamma_e} + \frac{(gq'_r)^2}{2(\Gamma_s - \Gamma_e)}, \quad (27)$$

one finds

$$\frac{\partial E_p}{\partial t} + \nabla \cdot [\mathbf{u}(E_p + \phi)] - V_T \frac{\partial}{\partial z} \left[\frac{(gq'_r)^2}{2(\Gamma_s - \Gamma_e)} \right] = 0. \quad (28)$$

One can also arrive at the quadratic energy equation in (28) from (8) by using the decompositions $\theta_e = \tilde{\theta}_e + \theta'_e$ and $q_t = \tilde{q}_t + q'_t$ and then manipulating the corresponding equations (not shown).

As in the other cases above, this energy E_p offers insight into the stability condition. As mentioned above, the difference $\Gamma_s - \Gamma_e$ is positive for decreasing profile of saturation water vapor. Therefore, for $B_{vs} < 0$, the condition $\Gamma_e > 0$ gives a positive definite energy and is a sufficient condition for stability when $V_T > 0$. Note that this stability condition for $V_T > 0$ is different from the stability condition for $V_T = 0$. Also, what is not clear from the form of E_p is a sufficient condition for instability, which will be explored next.

3. Linear instability analysis of a saturated environment

While the energetics in section 2 offers some insight into stability boundaries, it does not fully characterize instability boundaries. In particular, a more detailed linear instability analysis is needed to analyze how finite rainfall speed $V_T > 0$ affects the stability. As in Emanuel (1986), we consider the simplest case of periodic boundary conditions and look for growing solutions to the system (14) and (15). Here, we focus on stability/instability boundaries.

a. Eigenvalue problem and characteristic polynomial

Starting from (14) and (15) and assuming $\Gamma_e \neq 0$, it is convenient to introduce the rescaled variables

$$\Theta_e = \frac{g}{\theta_o} \frac{\theta'_e}{|\Gamma_e|^{1/2}}, \quad \text{and} \quad Q = \frac{gq'_t}{(\Gamma_s - \Gamma_e)^{1/2}}. \quad (29)$$

We note again that $\Gamma_s - \Gamma_e$ is always positive, but Γ_e may be negative in physically relevant parameter regimes. Written in terms of the new variables in (29), the linearized equations become

$$\frac{\partial \mathbf{u}'}{\partial t} = -\mathbf{V}\phi + \hat{\mathbf{k}}[|\Gamma_e|^{1/2}\Theta_e - (\Gamma_s - \Gamma_e)^{1/2}Q],$$

$$\nabla \cdot \mathbf{u}' = 0 \quad \text{and} \quad (30)$$

$$\frac{\partial \Theta_e}{\partial t} + \text{sign}(\Gamma_e)|\Gamma_e|^{1/2}w' = 0,$$

$$\frac{\partial Q}{\partial t} - (\Gamma_s - \Gamma_e)^{1/2}w' - V_T \frac{\partial Q}{\partial z} = 0. \quad (31)$$

Periodic boundary conditions allow for solutions of the form $(\cdot)(\mathbf{x}, t; \mathbf{k}) = (\cdot)(\mathbf{k}) \exp\{i[\mathbf{k} \cdot \mathbf{x} - \sigma(\mathbf{k})t]\}$ with wavevector $\mathbf{k} = (k_x, k_y, k_z)$. After taking the divergence of the momentum equation in (30) and using the continuity condition, a Fourier transform yields

$$\hat{\phi} = -\frac{ik_z}{k^2}|\Gamma_e|^{1/2}\hat{\Theta}_e + \frac{ik_z}{k^2}(\Gamma_s - \Gamma_e)^{1/2}\hat{Q}. \quad (32)$$

Derivation of the remaining Fourier coefficients follows from substitution of (32) into the Fourier transforms of the momentum equation in (30) and (31):

$$-i\sigma\hat{u} = -ik_x\hat{\phi} = \frac{-k_x k_z |\Gamma_e|^{1/2}}{k^2}\hat{\Theta}_e + \frac{k_x k_z}{k^2}(\Gamma_s - \Gamma_e)^{1/2}\hat{Q},$$

$$-i\sigma\hat{v} = -ik_y\hat{\phi} = \frac{-k_y k_z |\Gamma_e|^{1/2}}{k^2}\hat{\Theta}_e + \frac{k_y k_z}{k^2}(\Gamma_s - \Gamma_e)^{1/2}\hat{Q},$$

$$-i\sigma\hat{w} = -ik_z\hat{\phi} + |\Gamma_e|^{1/2}\hat{\Theta}_e - (\Gamma_s - \Gamma_e)^{1/2}\hat{Q} = \frac{k_h^2}{k^2}|\Gamma_e|^{1/2}\hat{\Theta}_e - \frac{k_h^2}{k^2}(\Gamma_s - \Gamma_e)^{1/2}\hat{Q},$$

$$-i\sigma\hat{\Theta}_e = -\text{sign}(\Gamma_e)|\Gamma_e|^{1/2}\hat{w}, \quad \text{and}$$

$$-i\sigma\hat{Q} = (\Gamma_s - \Gamma_e)^{1/2}\hat{w} + ik_z V_T \hat{Q}. \quad (33)$$

Slaving of \hat{u} , \hat{v} introduces a zero eigenvalue associated with the vortical mode. When $k_h \neq 0$, the equations for \hat{w} , $\hat{\Theta}_e$, \hat{Q} can be written in matrix form (indicated by square brackets):

$$\begin{bmatrix} 0 & ik_h k^{-1} |\Gamma_e|^{1/2} & -ik_h k^{-1} (\Gamma_s - \Gamma_e)^{1/2} \\ -i \text{sign}(\Gamma_e) k_h k^{-1} |\Gamma_e|^{1/2} & 0 & 0 \\ i(\Gamma_s - \Gamma_e)^{1/2} k_h k^{-1} & 0 & -k_z V_T \end{bmatrix} \begin{bmatrix} k k_h^{-1} \hat{w} \\ \hat{\Theta}_e \\ \hat{Q} \end{bmatrix} = \sigma \begin{bmatrix} k k_h^{-1} \hat{w} \\ \hat{\Theta}_e \\ \hat{Q} \end{bmatrix}. \quad (34)$$

For brevity, we do not show the special case $k_h = 0$. The matrix above is Hermitian when Γ_e is positive [$\text{sign}(\Gamma_e) = 1$]; hence, in this case, all eigenvalues are real, and the system is neutrally stable. For the general case, the characteristic polynomial is given by

$$(k^2 \sigma^3 + k_z V_T k^2 \sigma^2 - k_h^2 \Gamma_s \sigma - k_h^2 k_z V_T \Gamma_e) \sigma = 0, \quad (35)$$

where the zero eigenvalue was also included.

b. Eigenmodes

To make a connection to the eigenmodes of the dry dynamics, we first consider the special case $V_T = 0$ and $k_h \neq 0$, and then the precipitating case $V_T > 0$ will be considered.

For $V_T = 0$, and in the case $k_h \neq 0$, the four eigenvalues are

$$\sigma^{0,q} = 0, \sigma^\pm = \pm \frac{k_h}{k} \Gamma_s^{1/2}. \quad (36)$$

The four eigenmodes of (33) are five-component vectors $(\hat{u}, \hat{v}, \hat{w}, \hat{\Theta}_e, \hat{Q})$. The eigenmodes corresponding to (36) are

$$\phi^0 = k_h^{-1} \begin{bmatrix} -k_y \\ k_x \\ 0 \\ 0 \\ 0 \end{bmatrix},$$

$$\phi^q = (\Gamma_s - \Gamma_e + |\Gamma_e|)^{-1/2} \begin{bmatrix} 0 \\ 0 \\ 0 \\ (\Gamma_s - \Gamma_e)^{1/2} \\ |\Gamma_e|^{1/2} \end{bmatrix}, \quad \text{and} \quad (37)$$

$$\phi^\pm = k^{-1} |\Gamma_s|^{1/2} (\Gamma_s - \Gamma_e + |\Gamma_s| + |\Gamma_e|)^{-1/2} \times \begin{bmatrix} ik_x k_z k_h^{-1} \\ ik_y k_z k_h^{-1} \\ -ik_h \\ \mp k \text{sign}(\Gamma_e) |\Gamma_e|^{1/2} \Gamma_s^{-1/2} \\ \pm k (\Gamma_s - \Gamma_e)^{1/2} \Gamma_s^{-1/2} \end{bmatrix}. \quad (38)$$

Comparing to the dry dynamics, $\sigma^0 = 0$, ϕ^0 can be identified with the zero-frequency vortical mode. The eigenvalues σ^\pm in (36) have the same form as the gravity waves frequencies of the dry, stratified case, but there is a stability boundary at $\Gamma_s = 0$: for $\Gamma_s > 0$, there are two neutrally stable, propagating modes; for $\Gamma_s < 0$, there is

one growing mode and one decaying mode. There is an additional zero eigenvalue $\sigma^q = 0$ and eigenmode ϕ^q associated with potential temperature and rainwater fluctuations.

For $V_T > 0$, the solution to the characteristic polynomial is nontrivial, and V_T plays a central role in the structure of the eigenmodes. Assuming the most general case $\Gamma_e \neq 0, \Gamma_s \neq 0, \Gamma_s - \Gamma_e \neq 0, k_h \neq 0, k_z \neq 0$, the vortical mode is the only eigenfunction with zero eigenvalue $\sigma^0 = 0$, and the vortical eigenmode ϕ^0 is given by (37). In addition, there are three more eigenvalues given by the cubic polynomial

$$k^2 \sigma^3 + k_z V_T k^2 \sigma^2 - k_h^2 \Gamma_s \sigma - k_h^2 k_z V_T \Gamma_e = 0 \quad (39)$$

[see (35)]. The corresponding eigenvectors are

$$\phi^{q,\pm} = \{k^2 + k_h^2 [|\Gamma_e| |\sigma^{q,\pm}|^{-2} + (\Gamma_s - \Gamma_e) |\sigma^{q,\pm} + k_z V_T|^{-2}]\}^{-1/2} \times \begin{bmatrix} ik_x k_z k_h^{-1} \\ ik_y k_z k_h^{-1} \\ -ik_h \\ -k_h (\sigma^{q,\pm})^{-1} \text{sign}(\Gamma_e) |\Gamma_e|^{1/2} \\ k_h (\sigma^{q,\pm} + k_z V_T)^{-1} (\Gamma_s - \Gamma_e)^{1/2} \end{bmatrix}, \quad (40)$$

where the superscript q,\pm makes sense, since the eigenvalues $\sigma^{q,\pm}$ and the eigenmodes $\phi^{q,\pm}$ given by (40) converge to the $V_T = 0$ expressions given by (36), (37), and (38).

In addition to the special case when $V_T = 0, k_h \neq 0$, one can also compute the eigenvalues and eigenvectors for the other special cases, such as $k_z = 0, \Gamma_e - \Gamma_s = 0$, but we will not present those cases for the sake of brevity.

For the case of (39) and (40), there is a real eigenvalue defining a neutrally stable mode that propagates, and there are two more eigenvalues that could be real or could be complex conjugates. In other words, these last two eigenmodes could be both neutrally stable or could be a stable/unstable pair, depending on the specific values of $\Gamma_e, \Gamma_s, V_T, k_h$, and k_z .

c. Numerical results

To further probe the stability and instability, we now turn to numerical computations of the eigenvalues from (39). Of particular interest are the $V_T > 0$ cases, for which the instability properties are not as easily deduced analytically.

The behavior for varying V_T and horizontal wavenumber k_h is illustrated in Fig. 2. The growth rate is

plotted versus horizontal wavenumber using fixed vertical wavenumber $k_z = 2\pi/15 \text{ km}^{-1}$, potential temperature gradient $B = 3 \text{ K km}^{-1}$, and saturation profile gradient $B_{vs} = -1.28 \text{ g kg}^{-1} \text{ km}^{-1}$. The horizontal wavenumber k_h has been scaled by $2\pi/40\,000 \text{ km}^{-1}$, and V_T has the realistic values $V_T = 0.5, 1, 1.5, 2, \dots, 5 \text{ m s}^{-1}$ (Rogers and Yau 1989). When the rainfall speed is small, the instabilities occur in a finite band of smaller horizontal wavenumbers (larger horizontal scales). As V_T increases, instabilities appear at increasingly smaller scales, but the growth rate appears to saturate. Qualitatively similar behavior is observed for growth rate versus total wavenumber and for growth rate versus k_z for fixed k_h (not shown). While it is unclear whether the large-scale unstable modes have physical significance, instability arises on scales of 50 km and smaller for reasonable values of V_T (larger than roughly 0.6 m s^{-1}) and may be relevant for the growth of individual cumulus clouds.

Figure 3 shows the (in)stability regions in the $k_h (2\pi/40\,000 \text{ km}^{-1})$ versus B_{vs} plane for $V_T = 0$ (left), $V_T = 0.01$ (middle left), $V_T = 1$ (middle right), and $V_T = 10 \text{ m s}^{-1}$ (right). The gray region denotes the unstable scales. The dashed line $\Gamma_e = 0$ clearly separates

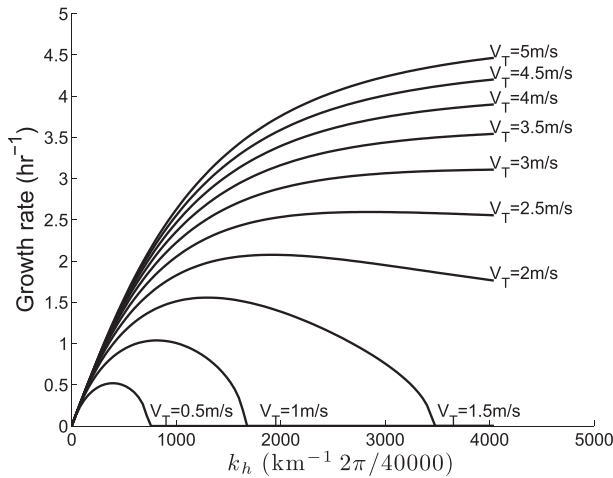


FIG. 2. Growth rates $\text{Im}(\sigma)$ of the unstable eigenmode as a function of k_h ($2\pi/40\,000\text{ km}^{-1}$) for $V_T = 0.5, 1.0, 1.5, 2, \dots, 5\text{ m s}^{-1}$, $k_z = 2\pi/15\text{ km}^{-1}$, $B = 3\text{ K km}^{-1}$, and $B_{vs} = -1.28\text{ g kg}^{-1}\text{ km}^{-1}$.

regions where all scales are stable from those where instabilities arise either in a finite band or at all scales. As the rainfall speed increases, the unstable region approaches the dashed line $\Gamma_e = 0$. This suggests that $\Gamma_e = 0$ is the stability boundary of the FARE model in saturated regions as $V_T \rightarrow \infty$. The other extreme limit $V_T \rightarrow 0$ appears to be a singular limit, in the sense that there is a qualitative change between $V_T = 0$ and $V_T \rightarrow 0$ [see also (19) in Emanuel (1986)]. The insert in the middle-left panel of Fig. 3 shows a zoom at large scales, where, for $V_T = 0.01\text{ m s}^{-1}$, we verify that instabilities occur at large scales provided that $\Gamma_e < 0$. Our numerical calculations indicate that for any positive V_T and $\Gamma_e < 0$, there will be instabilities at large-enough scales (perhaps larger than planetary scales). On the other hand, the limiting case $V_T = 0$ has all scales stable if $\Gamma_s > 0$ and all scales unstable if $\Gamma_s < 0$.

The conditional nature of the instabilities shown here is perhaps better understood in the $(B_{vs} = dq_{vs}/dz,$

$B = d\tilde{\theta}/dz)$ plane, allowing both B_{vs} and B to change. We let B vary about the standard value of 3 K km^{-1} . Although it is much harder to identify a typical B_{vs} , we use values close to a decrease of 20 g kg^{-1} over 15 km . Figure 4 shows the stability regions for $V_T = 0$ (left), $V_T = 0.05$ (middle left), $V_T = 5$ (middle right), and $V_T = 1000\text{ m s}^{-1}$ (right). In each panel, the dashed line is $\Gamma_e = 0$, and the solid line is $\Gamma_s = 0$. In the left panel with $V_T = 0$, we clearly identify Γ_s to be the stability parameter. In the right panel with $V_T = 1000\text{ m s}^{-1}$ very large, Γ_e replaces Γ_s as the stability boundary. As indicated by the middle-left panel with very small but positive $V_T = 0.05\text{ m s}^{-1}$, the region where $\Gamma_s > 0, \Gamma_e < 0$ is unstable at large horizontal scales but stable at small horizontal scales (1 km). In other words, for small V_T , the large scales become unstable in the region where the equivalent potential temperature background decreases with height, and the small scales become unstable close to the $\Gamma_s = 0$ region. On the other hand, $V_T = 0$ makes the large horizontal scales stable in the middle strip, indicating that $V_T = 0$ is a singular limit. The middle-right panel shows that for moderate values of V_T , there can be a finite wavenumber band of instabilities or instability at all horizontal wavenumber, depending on the values of B and B_{vs} .

Figure 5 helps to further analyze the effect of rainfall speed for the creation of instabilities. For fixed $B = 3\text{ K km}^{-1}$, the figure shows the (in)stability regions as a function of $B_{vs} = dq_{vs}/dz$ and V_T , with solid line to denote $\Gamma_s = 0$ (stability interface when $V_T = 0$; $B_{vs} \approx -1.37\text{ g kg}^{-1}\text{ km}^{-1}$), and with dashed line to denote $\Gamma_e = \Gamma_s + gB_{vs} = 0$ ($B_{vs} \approx -1.206\text{ g kg}^{-1}\text{ km}^{-1}$). One can see that $\Gamma_e > 0$ is a sufficient condition for stability. The region $\Gamma_e < 0$ has unstable modes and is divided into three subregions: (dark gray) the region with instabilities at both $k_h = 2\pi\text{ km}^{-1}$ (small scales) and $k_h = 2\pi/40\,000\text{ km}^{-1}$ (large scales); (gray) the region with instabilities at large scales; and (light gray) the region with no instabilities for these scales. The zoom to small

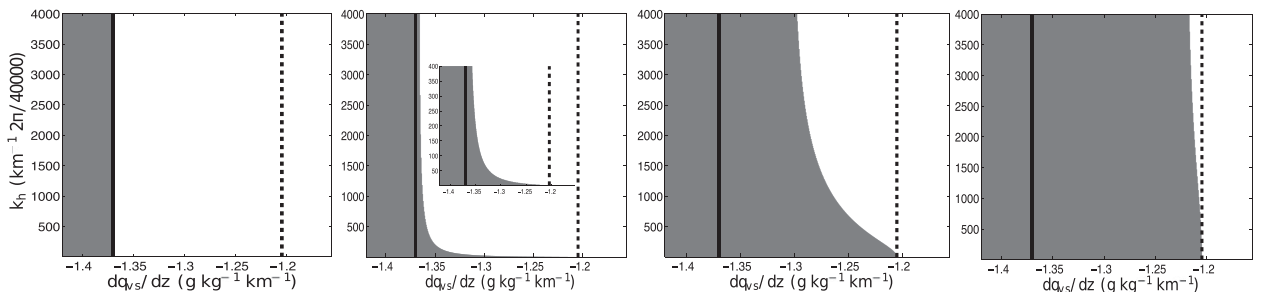


FIG. 3. Stability regions in the B_{vs} vs k_h ($2\pi/40\,000\text{ km}^{-1}$) plane for (left)–(right) $V_T = 0, 0.01, 1,$ and 10 m s^{-1} . The values $k_z = 2\pi/15\text{ km}^{-1}$ and $B = 3\text{ K km}^{-1}$ are fixed. The gray region denotes the unstable scales. The dashed vertical line indicates $\Gamma_e = 0$, and the solid vertical line indicates $\Gamma_s = 0$. The middle-left panel also includes a plot with truncated values of k_h from 1 to 400 ($2\pi/40\,000\text{ km}^{-1}$).

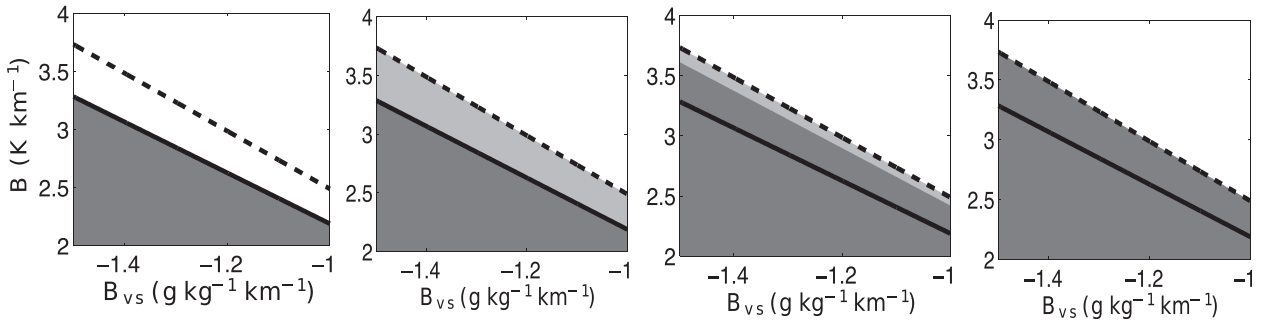


FIG. 4. Stability regions in the $(B_{vs} = dq_{vs}/dz, B = d\tilde{\theta}/dz)$ plane for (left)–(right) $V_T = 0, 0.05, 5,$ and 1000 m s^{-1} . The dashed line is $\Gamma_e = 0$, and the solid line is $\Gamma_s = 0$. The light gray region indicates instabilities at large scales (chosen to be identified by the planetary scale $40\,000 \text{ km}$); the dark gray region indicates instabilities at both large and small scales (1 km); the white region indicates no instabilities at these scales.

values of V_T in the right panel is necessary to see that the stability curve for scales smaller than Earth’s circumference starts at $\Gamma_s = 0$ for $V_T \rightarrow 0$ and asymptotically approaches $\Gamma_e = 0$ for V_T large. Increasing rainfall speed changes the linear instability interface from $\Gamma_s = 0$ for $V_T = 0$ to $\Gamma_e = 0$ as V_T increases.

Explicit expressions for the eigenvalues in the two extreme cases $V_T = 0$ and $V_T \rightarrow \infty$ reveal two stability parameters. The wave modes have a frequency of $\sigma^\pm = \pm(k_h/k)\Gamma_s^{1/2}$ and $\sigma^\pm = \pm(k_h/k)\Gamma_e^{1/2}$ for these two extreme cases, respectively. This shows that the gradient Γ_s controls stability in nonprecipitating environments, while the parameter Γ_e replaces Γ_s for fast precipitation when $V_T \rightarrow \infty$. (See section 4 for more discussion of the limit $V_T \rightarrow \infty$; also, for comparison, recall that the frequencies are $\sigma^\pm = \pm(k_h/k)\Gamma_v^{1/2}$ in the unsaturated case, where Γ_v is derived from the virtual potential temperature θ_{vs} .) A transition from one extreme to the other is shown

in Fig. 6 for the unstable region with $\Gamma_s < 0$, displaying growth rates as a function of horizontal wavenumber and various values of V_T (fixed $B_{vs} = 1.4 \text{ g kg}^{-1} \text{ km}^{-1}$, $B = 3 \text{ K km}^{-1}$, and $k_z = 2\pi/15 \text{ km}^{-1}$). The thick dashed and solid lines are curves proportional to k_h/k as a function of k_h , with constants of proportionality $|\Gamma_s|^{1/2}$ and $|\Gamma_e|^{1/2}$, respectively. The intermediate curves correspond to finite values of V_T , where $V_T = 20 \text{ m s}^{-1}$ is already close to the limiting curve.

4. Asymptotic analysis in saturated environments for $V_T \rightarrow \infty$

Beyond the numerical indications of the $V_T \rightarrow \infty$ limit, a limiting system of equations can also be derived analytically. Here, we consider the nonlinear FARE model [(5)–(7)] in saturated environments and for rainfall speed $V_T \rightarrow \infty$ much larger than any other

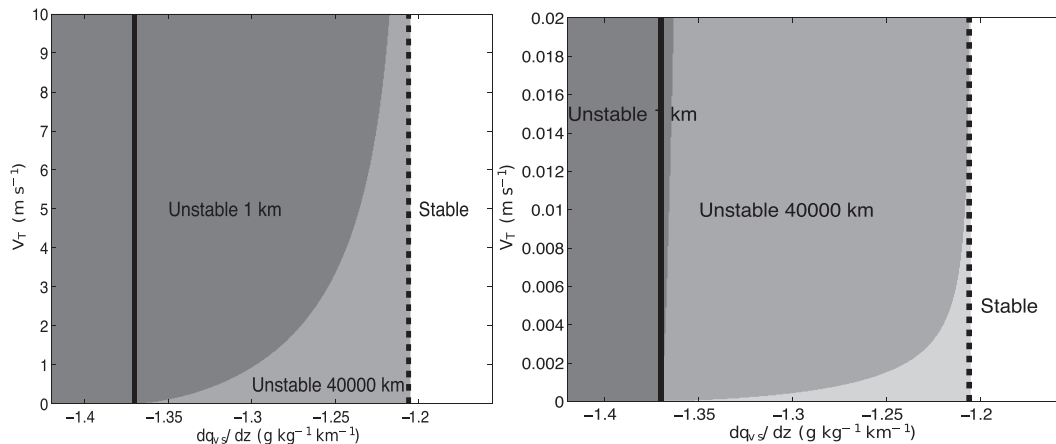


FIG. 5. (In)stability regions in the $(B_{vs} = dq_{vs}/dz, V_T)$ plane for $k_z = 2\pi/15 \text{ km}^{-1}$, $B = 3 \text{ K km}^{-1}$, and $B_{vs} \in [-1.42, -1.156] \text{ g kg}^{-1} \text{ km}^{-1}$: (left) $V_T \in [0, 10] \text{ m s}^{-1}$; (right) $V_T \in [0, 0.02] \text{ m s}^{-1}$. The dark (medium) gray region indicates the presence of unstable modes for horizontal wavenumbers $k_h = 2\pi \text{ km}^{-1}$ ($k_h = 2\pi/40\,000 \text{ km}^{-1}$). The light gray region in (right) indicates the area where no instabilities were found for $k_h \geq 2\pi/40\,000 \text{ km}^{-1}$. The solid line denotes $\Gamma_s = 0$, and the dashed line denotes $\Gamma_e = 0$. The white strip ($\Gamma_e > 0$) is the area with only stable modes.

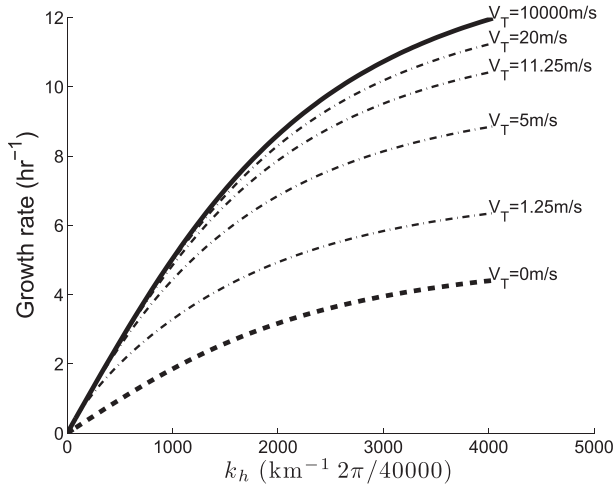


FIG. 6. Growth rates as a function of horizontal wavenumber for $dq_{vs}/dz = -1.4 \text{ g kg}^{-1} \text{ km}^{-1}$ and various values of V_T from 0 to $10\,000 \text{ m s}^{-1}$. The value of dq_{vs}/dz in this figure belongs to the unstable regime $\Gamma_s < 0$; $k_z = 2\pi/15 \text{ km}^{-1}$; and $B = 3 \text{ K km}^{-1}$.

velocity scale in the system. With characteristic length scale L and nonlinear time scale T and denoting non-dimensional quantities with an asterisk, the equations for the fluctuating fields become

$$\frac{\partial \mathbf{u}^*}{\partial t^*} + \mathbf{u}^* \cdot \nabla^* \mathbf{u}^* = -\nabla^* \phi^* + \hat{\mathbf{k}}(\theta_e^* - q_r^*), \quad (41)$$

$$\nabla^* \cdot \mathbf{u}^* = 0 \quad \text{and}$$

$$\frac{\partial \theta_e^*}{\partial t^*} + \mathbf{u}^* \cdot \nabla^* \theta_e^* = -\Gamma_e^* w^*,$$

$$\frac{\partial q_r^*}{\partial t^*} + \mathbf{u}^* \cdot \nabla^* q_r^* = V_T^* \frac{\partial q_r^*}{\partial z^*} + (\Gamma_s^* - \Gamma_e^*) w^*, \quad (42)$$

where $\mathbf{u}^* = (T/L)\mathbf{u}$, $\phi^* = (T^2/L^2)\phi$, $\theta_e^* = gT^2\theta_e/(L\theta_o)$, $q_r^* = gT^2q_r/L$, $\Gamma_e^* = T^2\Gamma_e$, $\Gamma_s^* = T^2\Gamma_s$, and $V_T^* = (T/L)V_T$.

Assuming that the velocity scale L/T , Γ_e^* , and $\Gamma_s^* - \Gamma_e^*$ are $O(1)$, let us analyze the asymptotic behavior of the solution as $V_T^* = \varepsilon^{-1} \rightarrow \infty$. All variables are assumed to admit the following expansion: $(\cdot)^* = (\cdot)_0 + (\cdot)_1\varepsilon + (\cdot)_2\varepsilon^2 + \dots$. Collecting $O(\varepsilon^{-1})$ terms in (41) and (42), it immediately follows that $\partial q_{r,0}^*/\partial z^* = 0$, which implies $q_{r,0}^* = q_{r,0}^*(\mathbf{x}_h^*, t)$ does not depend on height. Also assuming that rain fluctuations vanish at high-enough altitude in a column of saturated air leads to the conclusion that $q_{r,0}^* = 0$. Collecting $O(1)$ terms in the second equation of (42), we obtain a diagnostic equation for the $O(\varepsilon)$ rainwater fluctuation in terms of the $O(1)$ vertical velocity: $\partial q_{r,1}^*/\partial z^* = (\Gamma_s^* - \Gamma_e^*)w_0^*$. Collecting the remaining $O(1)$ terms, we find a closed system for the leading-order dynamics:

$$\frac{\partial \mathbf{u}_0^*}{\partial t^*} + \mathbf{u}_0^* \cdot \nabla^* \mathbf{u}_0^* = -\nabla^* \phi_0^* + \hat{\mathbf{k}}\theta_{e,0}^*,$$

$$\nabla^* \cdot \mathbf{u}_0^* = 0 \quad \text{and} \quad (43)$$

$$\frac{\partial \theta_{e,0}^*}{\partial t^*} + \mathbf{u}_0^* \cdot \nabla^* \theta_{e,0}^* = -\Gamma_e^* w_0^*. \quad (44)$$

In dimensional units, the leading-order terms are (dropping subscripts and assuming $q_{r,0}^* = 0$)

$$\frac{D\mathbf{u}}{Dt} = -\nabla\phi + \hat{\mathbf{k}}\frac{g\theta'_e}{\theta_o}, \quad \nabla \cdot \mathbf{u} = 0, \quad \frac{D}{Dt}\frac{g\theta'_e}{\theta_o} = -\Gamma_e w. \quad (45)$$

The limiting equation [(45)] has the conserved energy

$$E_0 = \frac{1}{2}\|\mathbf{u}\|^2 + \frac{(g\theta'_e/\theta_o)^2}{2\Gamma_e}, \quad (46)$$

which indicates that Γ_e is the stability parameter. The nonzero eigenvalues for the corresponding linearized system are $\sigma = \pm(k_h/k)\Gamma_e^{1/2}$.

The stability parameter obtained for asymptotic solutions as $V_T \rightarrow \infty$ in the FARE model coincides with the numerical evidence presented in section 3: namely, the sign of the gradient of rescaled equivalent potential temperature determines stability for large V_T .

It is interesting to note a similarity with theories for convectively coupled equatorial waves (Emanuel et al. 1994; Neelin and Zeng 2000; Frierson et al. 2004; Stechmann and Majda 2006; Kiladis et al. 2009). In these theories, a “moist” phase speed $c_m = \sqrt{1 - \bar{Q}}$ is identified as a reduced phase speed compared to the “dry” phase speed $c_d = 1$. The moist phase speed c_m is associated with a moist stability parameter $1 - \bar{Q}$, which resembles a nondimensional version of $\Gamma_e = (g/\theta_o)d\tilde{\theta}_e/dz = (g/\theta_o)[d\tilde{\theta}/dz + (L/c_p)d\tilde{q}_v/dz]$, with the identifications of $1 \leftrightarrow d\tilde{\theta}/dz$ and $-\bar{Q} \leftrightarrow (L/c_p)d\tilde{q}_v/dz$. In the theories for convectively coupled equatorial waves, the reduced stability parameter $1 - \bar{Q}$ arises from an asymptotic assumption: convection is in a state of quasi equilibrium relative to the slowly varying, large-scale atmospheric circulation. In the present paper, interestingly, the reduced stability parameter Γ_e also arises from an asymptotic assumption: precipitation is fast ($V_T \rightarrow \infty$) relative to the time scales of atmospheric dynamics.

5. Concluding discussion

A linear stability analysis was presented for fluid dynamics with water vapor and precipitation, where the precipitation falls relative to the fluid at speed V_T . This system is an idealization of precipitating atmospheric convection, with a highly simplified representation of cloud microphysics. One aim was to bridge the two

TABLE 2. Summary of sufficient conditions for stability and instability for different cases of rainfall velocity V_T . For each case, the stability (instability) criterion is a positive (negative) vertical derivative d/dz of the quantity listed. Two quantities arise: equivalent potential temperature θ_e and saturated potential temperature θ_s , as defined in Table 1.

Case	Stability criterion	Instability criterion
$V_T = 0$	$d\theta_s/dz > 0$	$d\theta_s/dz < 0$
V_T finite	$d\theta_e/dz > 0$	$d\theta_e/dz < 0$
$V_T \rightarrow \infty$	$d\theta_e/dz > 0$	$d\theta_e/dz < 0$

extreme cases of V_T by considering the full range of V_T values: (i) $V_T = 0$, (ii) finite V_T , and (iii) the limit of infinitely fast V_T . These results are summarized in Table 2. A second aim was to identify the appropriate energy in each case and to relate the form of the energy to the stability conditions.

In the $V_T = 0$ case, a single boundary ($d\theta_s/dz = 0$) divides the stable conditions ($d\theta_s/dz > 0$) and the unstable conditions ($d\theta_s/dz < 0$). The quantity θ_s was here called the saturated potential temperature, and it was defined as $\theta_s = \theta_e - \theta_0 q_t$. This is an idealization of the stability condition that has been previously derived from a thermodynamic perspective {e.g., see the quantity N_m^2 defined by Emanuel [1994, Eq. (6.2.10)]}. The key point in this case is that, when $V_T = 0$, the criterion $d\theta_s/dz = 0$ is the single boundary that separates the stable and unstable conditions. An energy principle was also formulated for this case. The energy has the same form as for an unsaturated atmosphere, except the buoyancy frequency squared Γ_v (derived from θ_v) is replaced with Γ_s (derived from θ_s). We notice that although θ_v and θ_s have the same fluctuation in saturated conditions ($\theta'_v = \theta'_s = \theta'_e - \theta_0 q'_t$), their backgrounds $\bar{\theta}_v$ and $\bar{\theta}_s$ differ by $\theta_0 [\epsilon_o - L/(c_p \theta_o) + 1] q_{ws}(z)$.

In the finite $V_T > 0$ case, in contrast, separate sufficient conditions are identified for stability versus instability: stability for $d\theta_e/dz < 0$ versus instability for $d\theta_s/dz < 0$. The energy in this case was derived, and it is convex only if the stability parameter Γ_e (derived from θ_e) is positive.

Taken together, the results of these two cases ($V_T = 0$ and $V_T > 0$) show that the limit $V_T \rightarrow 0$ is a singular limit. Specifically, it is singular in the sense that the stability boundaries of the $V_T = 0$ case and the small- V_T case are fundamentally different. When $V_T = 0$, stability is guaranteed for $d\theta_s/dz > 0$; in contrast, for any $V_T > 0$, stability is guaranteed only under the more restrictive condition $d\theta_e/dz > 0$. Consequently, results that apply for a nonprecipitating atmosphere ($V_T = 0$) may not hold for a precipitating atmosphere ($V_T > 0$), and vice versa.

Finally, in the case of infinitely fast V_T , the single boundary $d\theta_e/dz = 0$ divides the stable conditions

($d\theta_e/dz > 0$) and the unstable conditions ($d\theta_e/dz < 0$). Asymptotics were used to derive a limiting system of equations from the original fluid dynamics equations, in the limit $V_T \rightarrow \infty$. The stability result follows from the limiting fluid dynamics equations, and it is illustrated in numerical results as well. Also, an energy equation is found, and the energy is guaranteed to be positive if and only if the stability parameter Γ_e (derived from θ_e) is positive.

The two extreme cases here ($V_T = 0$ and $V_T \rightarrow \infty$) are reminiscent of two important moist thermodynamic processes: the reversible process and the pseudoadiabatic process. In the reversible process, when liquid condensate is formed, it is carried upward with the parcel {see Xu and Emanuel [1989, their (1)]; Williams and Renno [1993, their (3)]; or Emanuel (1994, section 4.7)}. In other words, this is a case with $V_T = 0$. On the other hand, in the pseudoadiabatic process, when liquid condensate is formed, it is immediately removed from the parcel {see Xu and Emanuel [1989, their (2)]; Williams and Renno [1993, their (2)]; or Emanuel (1994, section 4.7)}. In other words, this is a case with $V_T \rightarrow \infty$. In these two cases, the buoyancy of a rising parcel is different because of the inclusion or neglect of condensate loading, which appears here as the q_t term of (1). In the hydrodynamic model here, the smallness of condensate loading was derived as a result of asymptotics in the limit of $V_T \rightarrow \infty$; such a result confirms that these parcel-theory concepts have analogs when fluid dynamics (and hence nonhydrostatic pressure gradients) are included.

In the identification of separate criteria for stability versus instability, the results here are reminiscent of the notion of conditional instability. In particular, conditional instability can be described as an atmospheric state where the lapse rate is stable with respect to the dry adiabatic lapse rates but unstable with respect to the moist adiabatic lapse rate. This notion is typically applied under unsaturated conditions, in which case a parcel must be brought to saturation in order to realize the moist instability; consequently, conditional instability can be described as a state of uncertainty with regard to stability (Sherwood 2000; Schultz et al. 2000). In the present paper, saturated conditions are assumed from the outset, which precludes a precise comparison; nevertheless, uncertainty is found with regard to stability: it is possible for an atmospheric state to meet neither the sufficient condition for stability ($d\theta_e/dz > 0$) nor the sufficient condition for instability ($d\theta_s/dz < 0$). Here, the uncertainty arises from the consideration of finite V_T , in contrast to the traditional notion of conditional instability defined in terms of either a reversible process ($V_T = 0$) or a pseudoadiabatic process ($V_T \rightarrow \infty$).

An interesting feature that arises for finite V_T is that the instability or stability is wavelength dependent. Specifically, when V_T is fixed at a finite value, Fig. 2 shows that some wavelengths can be stable while other wavelengths are unstable. [This can also be seen in Emanuel (1986).] In contrast, when V_T is zero or infinitely fast, either all wavelengths are unstable or all wavelengths are stable; and when parcel theory is considered, no notion of wavelength enters into the theory at all. It is possible that the wavelength dependence of the instability plays a role in the formation of structures within broad areas of precipitating clouds, such as mesoscale convective systems (MCSs; Houze 2004) for the case of deep convection or pockets of open cells (POCs; Stevens et al. 2005; VanZanten et al. 2005; Wood et al. 2008) for the case of boundary layer stratocumulus clouds.

Acknowledgments. The research of G. H. -D., L. M. S., and S. N. S. was partially supported by the NSF program Collaborations in Mathematical Geosciences under Grant NSF CMG-1025188. The research of S. N. S. is also partially supported by Grant NSF DMS-1209409.

REFERENCES

- Bretherton, C. S., 1987a: A theory for nonprecipitating moist convection between two parallel plates. Part I: Thermodynamics and “linear” solutions. *J. Atmos. Sci.*, **44**, 1809–1827, doi:10.1175/1520-0469(1987)044<1809:ATFNMCM>2.0.CO;2.
- , 1987b: Analytical solutions of Emanuel’s model of precipitating convection. *J. Atmos. Sci.*, **44**, 3355–3355, doi:10.1175/1520-0469(1987)044<3355:ASOEMO>2.0.CO;2.
- Deng, Q., L. M. Smith, and A. J. Majda, 2012: Tropical cyclogenesis and vertical shear in a moist Boussinesq model. *J. Fluid Mech.*, **706**, 384–412, doi:10.1017/jfm.2012.260.
- Emanuel, K. A., 1986: Some dynamical aspects of precipitating convection. *J. Atmos. Sci.*, **43**, 2183–2198, doi:10.1175/1520-0469(1986)043<2183:SDAOPC>2.0.CO;2.
- , 1994: *Atmospheric Convection*. Oxford University Press, 592 pp.
- , J. D. Neelin, and C. S. Bretherton, 1994: On large-scale circulations in convecting atmospheres. *Quart. J. Roy. Meteor. Soc.*, **120**, 1111–1143, doi:10.1002/qj.49712051902.
- Fovell, R. G., and P.-H. Tan, 2000: A simplified squall-line model revisited. *Quart. J. Roy. Meteor. Soc.*, **126**, 173–188, doi:10.1002/qj.49712656209.
- Frierson, D. M. W., A. J. Majda, and O. M. Pauluis, 2004: Large scale dynamics of precipitation fronts in the tropical atmosphere: A novel relaxation limit. *Commun. Math. Sci.*, **2**, 591–626, doi:10.4310/CMS.2004.v2.n4.a3.
- Garner, S. T., and A. J. Thorpe, 1992: The development of organized convection in a simplified squall-line model. *Quart. J. Roy. Meteor. Soc.*, **118**, 101–124, doi:10.1002/qj.49711850306.
- Grabowski, W. W., and P. K. Smolarkiewicz, 1996: Two-time-level semi-Lagrangian modeling of precipitating clouds. *Mon. Wea. Rev.*, **124**, 487–497, doi:10.1175/1520-0493(1996)124<0487:TTLSTM>2.0.CO;2.
- , and H. Morrison, 2008: Toward the mitigation of spurious cloud-edge supersaturation in cloud models. *Mon. Wea. Rev.*, **136**, 1224–1234, doi:10.1175/2007MWR2283.1.
- Hernandez-Duenas, G., A. J. Majda, L. M. Smith, and S. N. Stechmann, 2013: Minimal models for precipitating turbulent convection. *J. Fluid Mech.*, **717**, 576–611, doi:10.1017/jfm.2012.597.
- Houze, R. A., Jr., 1993: *Cloud Dynamics*. International Geophysics Series, Vol. 53, Academic Press, 573 pp.
- , 2004: Mesoscale convective systems. *Rev. Geophys.*, **42**, RG4003, doi:10.1029/2004RG000150.
- Kiladis, G. N., M. C. Wheeler, P. T. Haertel, K. H. Straub, and P. E. Roundy, 2009: Convectively coupled equatorial waves. *Rev. Geophys.*, **47**, RG2003, doi:10.1029/2008RG000266.
- Lipps, F. B., and R. S. Hemler, 1982: A scale analysis of deep moist convection and some related numerical calculations. *J. Atmos. Sci.*, **39**, 2192–2210, doi:10.1175/1520-0469(1982)039<2192:ASAOADM>2.0.CO;2.
- Majda, A. J., Y. Xing, and M. Mohammadian, 2010: Moist multi-scale models for the hurricane embryo. *J. Fluid Mech.*, **657**, 478–501, doi:10.1017/S0022112010001515.
- Moncrieff, M. W., 1981: A theory of organized steady convection and its transport properties. *Quart. J. Roy. Meteor. Soc.*, **107**, 29–50, doi:10.1002/qj.49710745103.
- , 1992: Organized convective systems: Archetypal dynamical models, mass and momentum flux theory, and parameterization. *Quart. J. Roy. Meteor. Soc.*, **118**, 819–850, doi:10.1002/qj.49711850703.
- , and J. S. A. Green, 1972: The propagation and transfer properties of steady convective overturning in shear. *Quart. J. Roy. Meteor. Soc.*, **98**, 336–352, doi:10.1002/qj.49709841607.
- , and M. Miller, 1976: The dynamics and simulation of tropical cumulonimbus and squall lines. *Quart. J. Roy. Meteor. Soc.*, **102**, 373–394, doi:10.1002/qj.49710243208.
- Morrison, H., and W. W. Grabowski, 2008a: Modeling supersaturation and subgrid-scale mixing with two-moment bulk warm microphysics. *J. Atmos. Sci.*, **65**, 792–812, doi:10.1175/2007JAS2374.1.
- , and —, 2008b: A novel approach for representing ice microphysics in models: Description and tests using a kinematic framework. *J. Atmos. Sci.*, **65**, 1528–1548, doi:10.1175/2007JAS2491.1.
- Neelin, J. D., and N. Zeng, 2000: A quasi-equilibrium tropical circulation model—Formulation. *J. Atmos. Sci.*, **57**, 1741–1766, doi:10.1175/1520-0469(2000)057<1741:AQETCM>2.0.CO;2.
- Ogura, Y., and N. Phillips, 1962: Scale analysis of deep and shallow convection in the atmosphere. *J. Atmos. Sci.*, **19**, 173–179, doi:10.1175/1520-0469(1962)019<0173:SAODAS>2.0.CO;2.
- Pauluis, O., 2008: Thermodynamic consistency of the anelastic approximation for a moist atmosphere. *J. Atmos. Sci.*, **65**, 2719–2729, doi:10.1175/2007JAS2475.1.
- , and J. Schumacher, 2010: Idealized moist Rayleigh–Bénard convection with piecewise linear equation of state. *Commun. Math. Sci.*, **8**, 295–319, doi:10.4310/CMS.2010.v8.n1.a15.
- Rogers, R., and M. Yau, 1989: *A Short Course in Cloud Physics*. 3rd ed. International Series in Natural Philosophy, Vol. 113, Butterworth–Heinemann, 304 pp.
- Schultz, D. M., P. N. Schumacher, and C. A. Doswell III, 2000: The intricacies of instabilities. *Mon. Wea. Rev.*, **128**, 4143–4148, doi:10.1175/1520-0493(2000)129<4143:TIOI>2.0.CO;2.
- Seifert, A., and K. D. Beheng, 2001: A double-moment parameterization for simulating autoconversion, accretion and selfcollection. *Atmos. Res.*, **59–60**, 265–281, doi:10.1016/S0169-8095(01)00126-0.
- , and —, 2006: A two-moment cloud microphysics parameterization for mixed-phase clouds. Part 1: Model description. *Meteor. Atmos. Phys.*, **92**, 45–66, doi:10.1007/s00703-005-0112-4.
- Seitter, K. L., and H.-L. Kuo, 1983: The dynamical structure of squall-line type thunderstorms. *J. Atmos. Sci.*, **40**, 2831–2854, doi:10.1175/1520-0469(1983)040<2831:TDSOSL>2.0.CO;2.

- Sherwood, S. C., 2000: On moist instability. *Mon. Wea. Rev.*, **128**, 4139–4142, doi:10.1175/1520-0493(2000)129<4139:OMI>2.0.CO;2.
- Spiegel, E., and G. Veronis, 1960: On the Boussinesq approximation for a compressible fluid. *Astrophys. J.*, **131**, 442–447, doi:10.1086/146849.
- Stechmann, S. N., and A. J. Majda, 2006: The structure of precipitation fronts for finite relaxation time. *Theor. Comput. Fluid Dyn.*, **20**, 377–404, doi:10.1007/s00162-006-0014-1.
- Stevens, B., 2005: Atmospheric moist convection. *Annu. Rev. Earth Planet. Sci.*, **33**, 605–643, doi:10.1146/annurev.earth.33.092203.122658.
- , G. Vali, K. Comstock, R. Wood, M. C. vanZanten, P. H. Austin, C. S. Bretherton, and D. H. Lenschow, 2005: Pockets of open cells and drizzle in marine stratocumulus. *Bull. Amer. Meteor. Soc.*, **86**, 51–57, doi:10.1175/BAMS-86-1-51.
- Sukhatme, J., A. J. Majda, and L. M. Smith, 2012: Two-dimensional moist stratified turbulence and the emergence of vertically sheared horizontal flows. *Phys. Fluids*, **24**, 036602, doi:10.1063/1.3694805.
- Vallis, G., 2006: *Atmospheric and Oceanic Fluid Dynamics: Fundamentals and Large-scale Circulation*. Cambridge University Press, 745 pp.
- VanZanten, M., B. Stevens, G. Vali, and D. Lenschow, 2005: Observations of drizzle in nocturnal marine stratocumulus. *J. Atmos. Sci.*, **62**, 88–106, doi:10.1175/JAS-3355.1.
- Williams, E., and N. Renno, 1993: An analysis of the conditional instability of the tropical atmosphere. *Mon. Wea. Rev.*, **121**, 21–36, doi:10.1175/1520-0493(1993)121<0021:AAOTCI>2.0.CO;2.
- Wood, R., K. Comstock, C. S. Bretherton, C. Cornish, J. Tomlinson, D. R. Collins, and C. Fairall, 2008: Open cellular structure in marine stratocumulus sheets. *J. Geophys. Res.*, **113**, D12207, doi:10.1029/2007JD009371.
- Xu, K.-M., and K. A. Emanuel, 1989: Is the tropical atmosphere conditionally unstable? *Mon. Wea. Rev.*, **117**, 1471–1479, doi:10.1175/1520-0493(1989)117<1471:ITTACU>2.0.CO;2.
- , and D. Randall, 2001: Updraft and downdraft statistics of simulated tropical and midlatitude cumulus convection. *J. Atmos. Sci.*, **58**, 1630–1649, doi:10.1175/1520-0469(2001)058<1630:UADSOS>2.0.CO;2.